

Research on Deep Learning Model of Feature Extraction Based on Convolutional Neural Network

Houze Liu¹, Iris Li², Yaxin Liang³, Dan Sun⁴, Yining Yang⁵, Haowei Yang⁶

¹New York University, Department Computer Science and Engineering, New York, USA, hl2979@nyu.edu

²New York University, Graduate School of Art & Science, New York, USA, irisepode@gmail.com

³University of Southern California, Viterbi School of Engineering, Los Angeles, USA, yaseen.liang@outlook.com

⁴Washington University, Department of Electrical and Systems Engineering, St. Louis, USA, sun.dan@wustl.edu

⁵Carnegie Mellon University, School of Computer Science, Pittsburgh, USA, yiningya@andrew.cmu.edu

⁶University of Houston, Cullen College Of Engineering, Houston, USA, yanghaowei09@gmail.com

Abstract—Neural networks with relatively shallow layers and simple structures may have limited ability in accurately identifying pneumonia. In addition, deep neural networks also have a large demand for computing resources, which may cause convolutional neural networks to be unable to be implemented on terminals. Therefore, this paper will carry out the optimal classification of convolutional neural networks. Firstly, according to the characteristics of pneumonia images, AlexNet and InceptionV3 were selected to obtain better image recognition results. Combining the features of medical images, the forward neural network with deeper and more complex structure is learned. Finally, knowledge extraction technology is used to extract the obtained data into the AlexNet model to achieve the purpose of improving computing efficiency and reducing computing costs. The results showed that the prediction accuracy, specificity, and sensitivity of the trained AlexNet model increased by 4.25 percentage points, 7.85 percentage points, and 2.32 percentage points respectively. The graphics processing usage has decreased by 51% compared to the InceptionV3 mode.

Keywords—Deep learning; image classification; convolutional neural network; diagnosis of pneumonia

I. INTRODUCTION

In the past diagnosis of pneumonia, the determination of images mostly relied on doctors with rich clinical practice experience, and this difference could not be guaranteed to be correct due to artificial experience. In recent years, computer-assisted imaging (CCAD) has been gradually applied in the

imaging field [1], and has become an important basis for doctors to evaluate image quality [2]. Researchers have classified the images of pneumonia images and given the corresponding algorithms [3]. Researchers have used a 121-level convolutional neural network to perform experiments on 112,120 labeled lung X-ray images, and found that 11 of them achieved results comparable to or better than imaging diagnoses by radiographers [4].

In this paper, the convolutional neural network based on knowledge extraction is optimized to enhance the identification performance of pneumonia. AlexNet with the initial version was selected [5]. This algorithm uses V3 and AlexNet as research modules to study the transfer learning-based neural network model to solve the overfitting problem caused by the small number of samples [6]. Further improve AlexNet's recognition performance while reducing GPU computing resource consumption [7].

II. PNEUMONIA IDENTIFICATION AND NETWORK COMPRESSION METHODS

A. Pneumonia classification network structure design

Firstly, this paper analyzes the current mainstream deep neural network architecture, including AlexNet, VGG16, ResNet18, ResNet34, InceptionV3, and so on [8]. The error rate, parameter number, network depth, and so on are compared [9].

TABLE I. COMPARISON OF PERFORMANCE OF EACH MODEL

Model name	Top-1 error rate /%	Network depth	Number of parameters /10 ⁶	Computation /10 ⁶
AlexNet	38.23	8	64.90	750
VGG16	25.73	24	144.06	15938
ResNet18	29.04	19	14.79	1875
ResNet34	22.43	35	25.21	3750
Inception V3	19.55	166	24.79	5208

Compared with other methods, Inception V3 model has obvious superiority in evaluating the Top-1 error rate of the discrimination accuracy index [10]. Compared with the existing AlexNet method, the false positive rate of this method

is reduced by nearly 1/2. Google introduced the Google Network Model in 2014, which includes five convolutional layers, three pooled layers, one fully connected layer, and 11 initial components [11]. As you can see from Table 1,

although the InceptionV3 schema has a network depth of about 20 AlexNet schemas, it has fewer than 38.5 million parameters due to its factored operation [12]. In the selection of teacher model, people should first consider the accuracy rate of pattern recognition, so this paper chooses "cognitive model" as the teacher model [13].

When selecting the student model, people should focus on the number of parameters required and the time required [14]. The number of parameters required is directly related to the storage capacity required, and the time required will also be greatly increased [15]. AlexNet is a deep neural network with 5 convolutional networks and 3 fully connected structures established by Hinton et al., University of Toronto, Canada, in 2012. AlexNet is computationally equivalent to 1/21 of V3 and VGG16. Although there is no special advantage in parameter quantization [16]. This project chooses AlexNet

mode as the research object in view of the shortcomings of GPU in computing performance in reality [17].

B. Data Compression in network Mode

Select InceptionV3, which has a more complex structure and a deeper layer, and AlexNet, which has a simpler structure and a shallower number of layers [18]. First of all, the independent study of the teacher to get a satisfactory effect, and then the study of the teacher [19]. Secondly, students are modeled and softmax is used to convert the obtained learning results into learning methods [20]. so as to enhance the learning effect of the learning object. In Figure 1, the teacher model InceptionV3 is "softened" with temperature parameter T, and then the softened probability distribution - soft target is obtained by softmax transformation (the picture is quoted in Appl.Sci. 2019, 9(10), 1966).

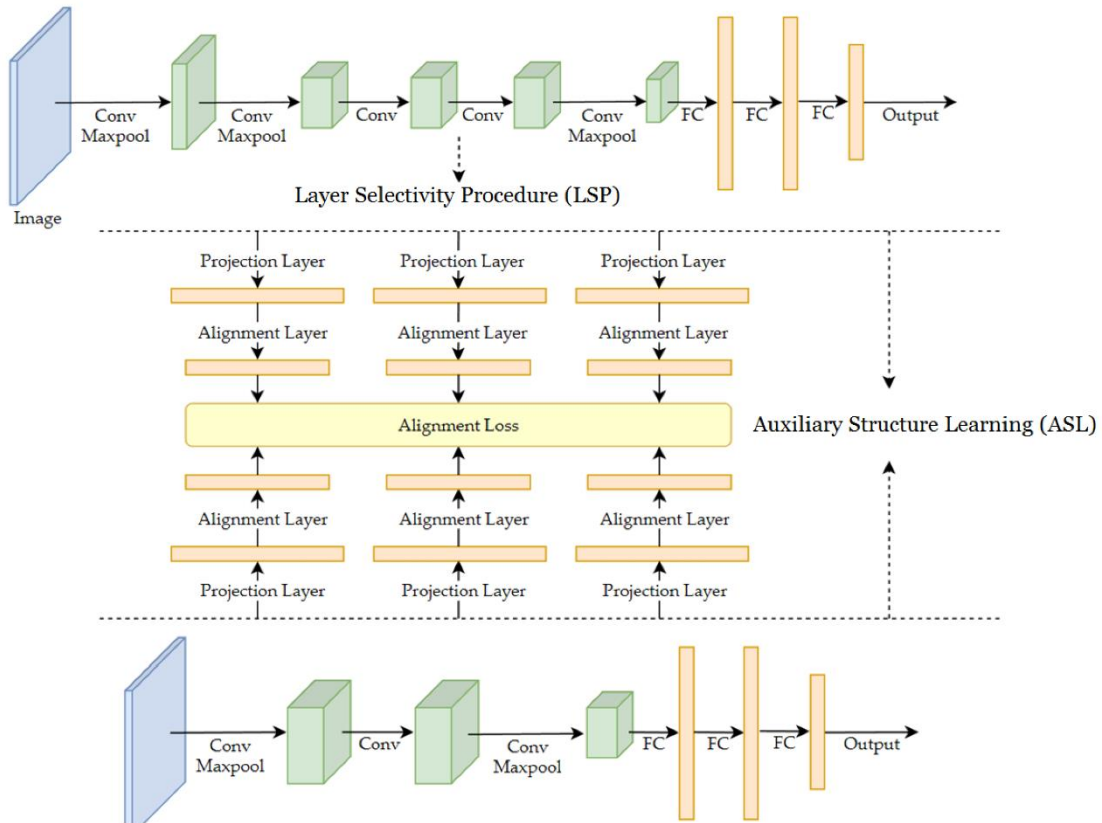


Fig. 1. Knowledge distillation network structure

This project intends to extract the "soft" object from the teacher's modeling, so as to effectively improve its identification performance [21]. In the learning phase, adjusting the value of parameter T is directly related to the learning effect, and usually takes an integer greater than 0. In this study, 1, 10, 20, 30, 40, and 50 were selected as experimental parameters, and their learning effects in T-size (Table 2) were compared [22]. When the parameter is set to 1, the accuracy, specificity, and sensitivity obtained are better than other options, so the adjustment parameter T is set to 1 in future learning [23].

TABLE II. EXPERIMENTAL RESULTS OF DIFFERENT PARAMETERS T

Parameter T	Accuracy rate /%	loss	Specificity /%	Sensitivity /%
1	95.83	0.003	88.06	99.96
10	95.18	0.021	87.19	99.98
20	93.89	0.037	83.31	99.98
30	93.24	0.054	81.15	99.45
40	92.26	0.068	80.29	99.45
50	90.00	0.121	78.57	99.45

C. Classification Process

This paper proposes an idea based on transfer learning, that is, after network training, all the training parameters are saved. The goal is to improve learning outcomes and reduce the probability of overlearning [24]. Initialize and learn parameters at the fully connected level. Finally, the effectiveness of the proposed algorithm is verified by simulation [25]. The method of "teaching" by the teacher is proposed to realize the learning of various parameters required in the modeling process of the teacher [26]. So that the whole small network has strong discernability [27]. Image steganography mainly extracts residual features from images by establishing residual models, and uses statistical models to strengthen features and combines machine learning methods to achieve classification. For an image of length m and width n , $U = \{U_{i,j}\} \in R^{m \times n}$, where the pixel value, $U_{i,j}$, ranges

$$\begin{bmatrix} Z_{i-1,j-1} & Z_{i,j-1} & Z_{i+1,j-1} \\ Z_{i-1,j} & Z_{i,j} & Z_{i+1,j} \\ Z_{i-1,j+1} & Z_{i,j+1} & Z_{i+1,j+1} \end{bmatrix} = \begin{bmatrix} U_{i-1,j-1} & U_{i,j-1} & U_{i+1,j-1} \\ U_{i-1,j} & U_{i,j} & U_{i+1,j} \\ U_{i-1,j+1} & U_{i,j+1} & U_{i+1,j+1} \end{bmatrix} + \begin{bmatrix} E_{i-1,j-1} & E_{i,j-1} & E_{i+1,j-1} \\ E_{i-1,j} & E_{i,j} & E_{i+1,j} \\ E_{i-1,j+1} & E_{i,j+1} & E_{i+1,j+1} \end{bmatrix} \quad (1)$$

The algorithm adds two hiding modes of $+1$ and -1 to the watermark, and its hiding probability is 0.5 , which is the same as the artificially added low frequency noise [28]. The proportion of steganography in the whole image is very small, so it needs to be preprocessed to reduce its interference to the image in order to obtain the densification characteristics. Fridrich et al. established a hidden detection depth modeling - Super resolution (SRM), which extracts the residual information of dense images by establishing the association between edge points and core points to obtain hidden information. The residual R_{res} is calculated by

$$R_{res} = \hat{Z}_{i,j} - \lambda Z_{i,j} \quad (2)$$

$\hat{Z}_{i,j}$ is the pixel, and the λ order predicted value of $Z_{i,j}$ is obtained from the pixels around $Z_{i,j}$. The relationships constructed in SRM include simple relationships in the pixel subtractive adjacency model and other complex relationships, respectively

$$\begin{aligned} R_{res} &= Z_{i,j+1} - Z_{i,j} \\ R_{res} &= (2Z_{i,j-1} - Z_{i-1,j-1} - Z_{i+1,j-1} + 2Z_{i+1,j}) - 4Z_{i,j} \end{aligned} \quad (3)$$

Residuals introduce a nonlinear relationship by selecting the smaller or larger value of the two-pixel relationships, thus improving the diversity of the image. For example, the amount of surplus is minimal both horizontally and vertically

$$\begin{aligned} R_{res} &= \min\{(Z_{i,j-1} + Z_{i,j+1} - 2Z_{i,j}), \\ &(Z_{i-1,j} + Z_{i+1,j} - 2Z_{i,j})\} \end{aligned} \quad (4)$$

In this method, truncation operation is used to define the residual interval, and it is convenient to describe the residual characteristics by co-existing matrix [29]. Quantization operation is used to enhance the hiding effect of

from 0 to 255. Embedded information is arbitrary multimedia information, which is converted into bit data stream steganography in an image carrier during embedding. The steganographic information is a matrix of the same size as the image U , $E = \{E_{i,j}\} \in R^{m \times n}$, and $E_{i,j} = \{0, -1, +1\}$. The encoding of steganographic information is extracted by comparing the original image and analyzing the location of pixel value change. Spatial adaptive steganography selects steganographic position $Q = \{(i_0, j_0), (i_1, j_1), \dots, (i_\sigma, j_\sigma)\}$ in an image by designing a distortion function and minimizing the calculated distortion value, where σ is the length of a stream of steganographic information bits in an image. The steganographic image is $Z = \{Z_{i,j}\} \in R^{m \times n}$, $Z = U + E$. For a 3×3 region in the image, the steganographic image consists of

watermarking, which makes the residual characteristics of the dense image and the picture have a big difference.

$$R_{res} = trunc_T \left(round \left(\frac{R_{res}}{c} \right) \right) \quad (5)$$

c is the step size of quantization, $c \in \{\lambda, 1.5\lambda, 2\lambda\}$ when $\lambda > 1$, and $c \in \{1, 2\}$; $round(\cdot)$ is an integer operation when $\lambda = 1$. $trunc_T(\cdot)$ is a truncated operation. The residual information extracted was statistically processed by the co-existence matrix. Use classical machine learning algorithms such as integrated classifiers to identify hidden images.

In A pixel region $U' \in R^{t \times t}$, $t \in \{t | t = 2k + 1, k \in Z\}$ of the carrier image, if the central pixel is, $U_{i,j}$, then the vector formed by the surrounding pixels is, $M_{i,j}^{U'}$, satisfying the condition, $M_{i,j}^{U'} \subset U', U_{i,j} \notin M_{i,j}^{U'}$. Suppose there is a linear function f which can obtain the C order value of the central pixel according to the surrounding pixels, $\lambda U_{i,j}$, namely

$$f(M_{i,j}^{U'}) = \lambda U_{i,j} \quad (6)$$

After the steganographic information E' is embedded in the carrier image region U' , it becomes steganographic image region Z' , the center pixel in the steganographic region, and the residual $res \in R$ of $Z_{i,j}$ is obtained by the difference between the surrounding pixels of the center pixel, the center pixels of order $M_{i,j}^{Z'}$ and λ , and $\lambda Z_{i,j}$ namely

$$R_{res} = R(M_{i,j}^{Z'}, Z_{i,j}) = f(M_{i,j}^{Z'}) - \lambda Z_{i,j} \quad (7)$$

From equation (1), it can be seen that the steganographic image in equation (7), $M_{i,j}^Z, Z_{i,j}$ Be composed of

$$\begin{aligned} M_{i,j}^Z &= M_{i,j}^{U'} + M_{i,j}^{E'} \\ Z_{i,j} &= U_{i,j} + E_{i,j} \end{aligned} \quad (8)$$

Given the linear property of the function f

$$\begin{aligned} R_{res} &= f(M_{i,j}^{U'} + M_{i,j}^{E'}) - \lambda(U_{i,j} + E_{i,j}) \\ &= f(M_{i,j}^{E'}) - \lambda E_{i,j} + f(M_{i,j}^{U'}) - \lambda U_{i,j} \end{aligned} \quad (9)$$

According to equation (6), the final residual value is

$$R_{res} = f(M_{i,j}^{E'}) - \lambda E_{i,j} \quad (10)$$

After difference processing, the residual property of carrier image is 0, while the residual property of noisy image is steganography. An image segmentation method based on residual error is proposed, which can improve the recognition rate of the object to be detected. Thirty high-pass filters are studied by SRM method [30]. The processing of image convolution is essentially the addition of pixel weights. In this method, first order residuals are extracted from the left edge, and then moved column by column according to the step size. Finally, residuals are obtained by adding each pixel point and corresponding weight, and the residuals are sorted according to the order of their regions to form a residuals map. The procedure for generating the residual Graph is shown in Figure 2 (Graph neural networks: A review of methods and applications).

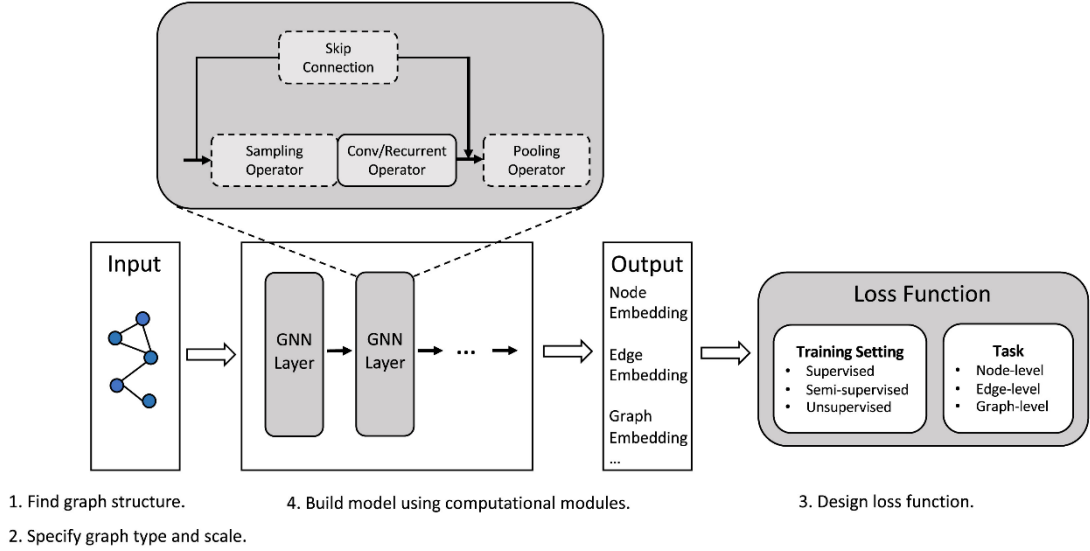


Fig. 2. Generation process of residual graph

A residual filter of size $k \times k$ performs image convolution in an image of size $m \times n$, and when there is no filling and the step size is $s \times s$, the size of the feature graph R is

$$\begin{aligned} R_{width} &= \frac{m-k}{s} + 1 \\ R_{length} &= \frac{n-k}{s} + 1 \end{aligned} \quad (11)$$

In the surrounding pixels of the center pixel, the adjacent pixels have the highest correlation with the center pixel, so the adjacent pixels are used to construct the residual extraction function. In order to prevent the introduction of image information and eliminate the excess $Z_{i,j}$ component of

$\lambda = \sum_p w_p$, the feature formula is transformed, that is

$$R_{res} = \sum_p w_p (Z_{i,j}^p - Z_{i,j}) \quad (12)$$

Where $Z_{i,j}^p - Z_{i,j}$ is the directional difference. The calculation of the residual can be converted into a linear combination of directional differences, and the parameter w_p of the linear combination is optimized according to the value. Parameter updating is achieved by introducing momentum, and the calculation process in pytorch deep learning framework is

$$w'_p = w_p - v l_k \quad (13)$$

v is the momentum, which is calculated by

$$v = \alpha v' + \frac{\partial L_{loss}}{\partial w_p} \quad (14)$$

III. EXPERIMENTAL DESIGN

A. Experimental Platform

This project takes PyTorch as the research object. PyTorch is a software for deep learning and deep neural networks, it uses PyTorch to construct neural networks, without writing all the execution methods, you can easily call the corresponding

function library. This will greatly shorten the learning cycle and improve the learning efficiency.

B. Data collection and preprocessing

The experimental dataset featured medical imagery captured from standard clinical examinations of individuals across various healthcare facilities. These images were made available in 2020 by Dieleman, an investigator affiliated with the University of California, San Diego, on the public repository Mendeley. Comprising 5915 chest X-ray photographs, the collection is stored in JPEG file format. The distribution of data is shown in Table 3.

TABLE III. DISTRIBUTION OF DATA SET COMPONENTS

Data type	Pneumonia.	Normal	Total
Training set	3922	1363	5285
Test set	394	236	630
total	4316	1599	5915

X-ray is the main evidence for clinical diagnosis of pneumonia, and the quality of the image is directly related to the diagnostic effect of the disease. Therefore, the collected image data are first screened by senior doctors to obtain high-quality images, and then the relevant professionals manually mark the images. The X-ray images were divided into two samples, which were manually labeled by two different pulmonary specialists. In order to prevent human labeling errors and ensure the accuracy of identification results,

different experts are used for labeling[31][32]. In order to meet the input requirements of the InceptionV3 and AlexNet modes, the size of the X-ray image is adjusted to the sizes of 299x299 and 224x224 pixels (Figure 3). The ratio of the number of X-ray images in the test set to the training set is approximately 1:10. In addition, the denoising problem also needs attention, and Yan's work has provided us with inspiration. By adopting unsupervised learning methods to deal with the denoising problem of Magnetic Resonance Imaging (MRI), Yan's research demonstrated the advanced application of deep learning technology in medical image processing [33]. By using a content encoder and a random noise encoder to separate the content information and noise in the image, and by regularizing the noise distribution through Kullback-Leibler (KL) divergence loss, it provides us with important references for optimizing our knowledge-extraction-based Convolutional Neural Network. Furthermore, combining adversarial loss and cycle consistency loss ensures the consistency of content information between noise input and denoised output images, which directly enlightens us on our goal to improve recognition performance while reducing the consumption of computational resources. Therefore, Yan's methodology not only technically supports our research but also offers us a new perspective on how to effectively utilize deep learning technology for processing medical images .

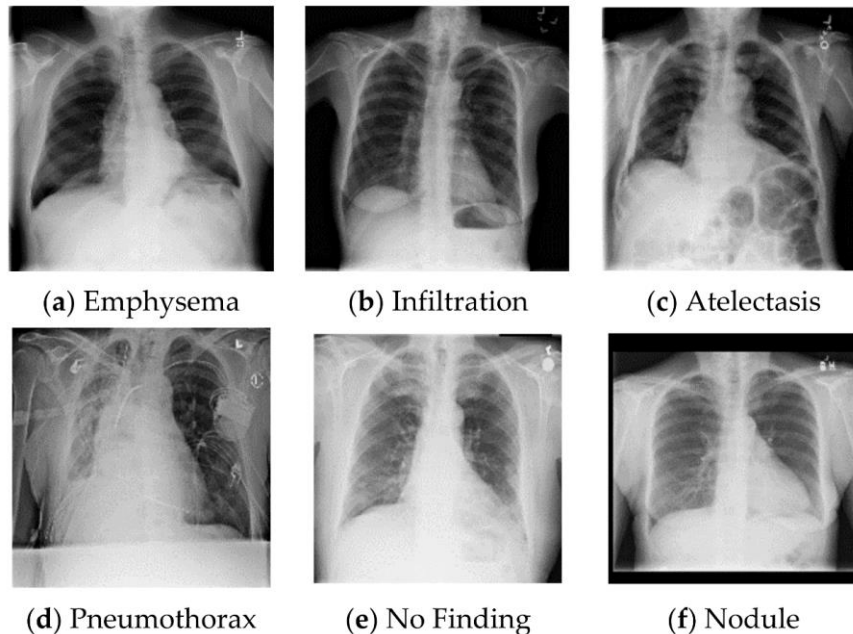


Fig. 3. Sample chest X-ray images

C. Parameter Settings

During the training of InceptionV3, a method based on transfer learning is used to initialize the parameters of the whole connectivity layer[34][35]. Set the learning rate to 5×10^{-3} , and set the decay rate to 0.9 and decay once during 7 epochs. With softmax function as the discriminant function and mutual entropy function as the damage function, the SGD

results are used to solve the problem[36]. At present, the most common algorithm is Adam algorithm, but this algorithm has a shortcoming, that is, the algorithm convergence speed is too fast, it is difficult to get the best. Through comparative test, the conclusion that SGD method is more effective is drawn. In AlexNet network training, the learning rate is set to 2×10^{-4} , the attenuation is 0.9, and the transfer learning algorithm similar

to V3 is used. The optimization method also adopts stochastic gradient descent algorithm[37].

D. Experimental process and results

This paper compares the common deep neural network models. In this model, the loss is a result of the amount of mutual entropy, which reflects the probability distribution between the predicted results and the actual data. Learning loss is often used to guide learning[38]. When it is less than 0.02, it indicates that the classifier has good learning performance. AlexNet, VGG16, ResNet18, ResNet34, Inception V3 were selected in this paper, and their recognition effects on the same training set and test set are shown in Table 4.

TABLE V. SYSTEM RESOURCE USAGE OF ALEXNET AND INCEPTION V3 MODELS

Model name	Video memory usage /GB	GPU usage /%	Training time /h
AlexNet	1.89	44.44	0.10
Inception V3	3.54	95.96	0.81

After the training, the difference of the performance of the optimized AlexNet (hereinafter referred to as AlexNet_S) model for pneumonia CT image classification was compared between the AlexNet model before optimization. The results show that the improved algorithm can not only improve the diagnosis of lung diseases, but also improve the specificity and sensitivity of indicators. In contrast, AlexNet_S mode is

TABLE VI. ALEXNET MODEL PERFORMANCE COMPARISON BEFORE AND AFTER OPTIMIZATION UNIT: %

Model name	Accuracy rate	specificity	sensitivity	GPU occupancy
Teacher Module	93.41	81.59	99.78	95.96
AlexNet	91.69	80.54	99.78	44.44
AlexNet_S	95.83	88.06	99.78	44.44

In contrast to the baseline AlexNet architecture, AlexNet_S achieved enhancements in the metric model's classification precision by 4.1 and 2.39 percentage points accordingly. The optimized model particularly excels in the initial detection of pneumonia; however, as its sensitivity rises, there is a concurrent reduction in the misclassification rate for pneumonia cases. Evaluation outcomes indicate that AlexNet_S surpasses the original AlexNet in terms of sensitivity and its sensitivity index closely mirrors that of the reference V3 model. Specificity is a key factor to evaluate the ability of this model to distinguish normal patients, and its high specificity can reduce the diagnostic error rate. In terms of specificity, AlexNet_S and InceptionV3 were 7.45% and 6.41 percentage points, respectively.

IV. CONCLUSION

This paper proposes a method to classify pneumonia CT images using convolutional neural networks. AlexNet and InceptionV3 neural networks with different structure and depth are used to obtain the optimal learning algorithm AlexNet_S which exceed InceptionV3. The enhancements in the AlexNet model, facilitated through the incorporation of knowledge extraction technology, have underscored the potential of deep learning techniques in medical image analysis. This approach not only addresses the limitations associated with deep neural networks' demand for computing resources but also sets a new benchmark for the

TABLE IV. RECOGNITION ACCURACY OF EACH MODEL

Model name	Accuracy rate /%	loss
AlexNet	94.552	0.006
VGG16	91.646	0.021
ResNet18	91.802	0.005
ResNet34	95.469	0.015
Inception V3	96.333	0.024

The recognition of the three modes with additional structure is much better in CT images. Therefore, this paper chooses the Teacher module with the initial V3 mode in the optimal algorithm, and takes AlexNet with less network structure as the learning module. The use of these two system resources was compared during the training (Table 5).

the student module, which can reduce the memory space by nearly half, which makes it more flexible to configure in a variety of computers with different memory capacities. At the same time, GPU utilization decreased by 51 percent, which allowed Student Module to run on computers with poor GPU performance, greatly improving neural network porting performance (Table 6).

implementation of efficient and effective diagnostic tools in medical imaging. Furthermore, our findings advocate for the continued exploration and development of optimized CNN models that can operate within the constraints of available computational resources while maintaining high standards of accuracy and efficiency. Such advancements hold the promise of revolutionizing the field of computer-assisted diagnostic imaging, making it more accessible, reliable, and cost-effective. Ultimately, this research paves the way for future studies to further refine these methods and explore their applicability across a broader spectrum of medical imaging tasks, potentially enhancing the diagnostic processes and patient outcomes in the realm of healthcare.

REFERENCES

- [1] Han, D., Chen, Y., Li, X., Li, W., Zhang, X., He, T., ... & Yu, N. Development and validation of a 3D-convolutional neural network model based on chest CT for differentiating active pulmonary tuberculosis from community-acquired pneumonia. *La radiologia medica*, vol. 128, pp. 68-80, January 2023.
- [2] Diao, S., Luo, W., Hou, J., Lambo, R., Al-Kuhali, H. A., Zhao, H., ... & Qin, W. Deep multi-magnification similarity learning for histopathological image classification. *IEEE Journal of Biomedical and Health Informatics*, vol. 27, pp.1535-1545, March 2023.
- [3] Weimin WANG, Yufeng LI, Xu YAN, Mingxuan XIAO, & Min GAO. (2024). Enhancing Liver Segmentation: A Deep Learning Approach with EAS Feature Extraction and Multi-Scale Fusion. *International Journal of Innovative Research in Computer Science & Technology*, 12(1), 26 - 34. Retrieved from <https://ijrcst.irpublications.org/index.php/ijrcst/article/view/21>

- [4] Chen, S., Lu, L., Zhang, Q., & Li, M. Optimal binomial reliability demonstration tests design under acceptance decision uncertainty. *Quality Engineering*, vol.32, pp. 492-508, March 2020.
- [5] Wang, X. S., Turner, J. D., & Mann, B. P. Constrained attractor selection using deep reinforcement learning. *Journal of Vibration and Control*, vol. 27, pp. 502-514, May 2021.
- [6] Praskatama, V., Sari, C. A., Rachmawanto, E. H., & Yaacob, N. M. PNEUMONIA PREDICTION USING CONVOLUTIONAL NEURAL NETWORK. *Jurnal Teknik Informatika (Jutif)*, vol. 4, pp.1217-1226, May 2023.
- [7] Yufeng Li, Weimin Wang, Xu Yan, Min Gao, & MingXuan Xiao. Research on the Application of Semantic Network in Disease Diagnosis Prompts Based on Medical Corpus. *International Journal of Innovative Research in Computer Science & Technology*, vol. 12, pp.1-9, February 2024.
- [8] Mann, P. S., Panchal, S. D., Singh, S., Saggi, G. S., & Gupta, K. A hybrid deep convolutional neural network model for improved diagnosis of pneumonia. *Neural Computing and Applications*, vol. 36, pp.1791-1804, April 2024.
- [9] Malik, H., Anees, T., Din, M., & Naeem, A. CDC_Net: Multi-classification convolutional neural network model for detection of COVID-19, pneumothorax, pneumonia, lung Cancer, and tuberculosis using chest X-rays. *Multimedia Tools and Applications*, vol. 82, pp.13855-13880, September 2023.
- [10] Yuying Liu;Zijian Zhao;Faliang Chang;Sanyuan Hu. An Anchor-Free Convolutional Neural Network for Real-Time Surgical Tool Detection in Robot-Assisted Surgery[J]. *IEEE Access*, vol. 8 2020. PP 78193-78201, September 2020.
- [11] Zhao Zijian,Cai Tongbiao,Chang Faliang,Cheng Xiaolin. Real-time surgical instrument detection in robot-assisted surgery using a convolutional neural network cascade.[J]. *Healthcare technology letters*, vol. 6 , Issue 6. 2019. PP 275-279, March 2019
- [12] Zijian Zhao,Sandrine Voros,Zhaorui Chen,Xiaolin Cheng. Surgical tool tracking based on two CNNs: from coarse to fine[J]. *The Journal of Engineering*, vol. 2019 , Issue 14. PP 467-472, September 2019.
- [13] Diganta Misra. Mish: A Self Regularized Non-Monotonic Neural Activation Function.[J]. *CoRR*, vol. 1908.08681 ,February 2019.
- [14] Armine Vardazaryan;Didier Mutter;Jacques Marescaux. Weakly-Supervised Learning for Tool Localization in Laparoscopic Videos.[J]. *Nicolas Padoy.CoRR*, vol. 1806.05573 ,July 2018.
- [15] Xu, H., Wen, S., Gimenez, A., Gamblin, T., & Liu, X. (2017, May). DR-BW: identifying bandwidth contention in NUMA architectures with supervised learning. In *2017 IEEE International Parallel and Distributed Processing Symposium (IPDPS)* (pp. 367-376). IEEE.
- [16] Twinanda Andru P,Shehata Sherif,Mutter Didier,Marescaux Jacques,de Mathelin Michel,Padoy Nicolas. EndoNet: A Deep Architecture for Recognition Tasks on Laparoscopic Videos.[J]. *IEEE transactions on medical imaging*, vol. 36 , Issue 1. 2017. PP 86-97, September 2017.
- [17] Saining Xie;Ross B. Girshick;Piotr Dollár;Zhuowen Tu;Kaiming He. Aggregated Residual Transformations for Deep Neural Networks. *CoRR*, vol. 1611.05431 ,March2016.
- [18] Jiahui Yu;Yuning Jiang;Zhangyang Wang;Zhimin Cao;Thomas S. Huang. UnitBox: An Advanced Object Detection Network. *CoRR*, vol. 1608.01471 ,January 2016.
- [19] Wei Liu;Dragomir Anguelov;Dumitru Erhan;Christian Szegedy;Scott E. Reed;Cheng-Yang Fu;Alexander C. Berg. SSD: Single Shot MultiBox Detector. *CoRR*, vol. 1512.02325 2015, April 2015.
- [20] Liu, Z., Yang, Y., Pan, Z., Sharma, A., Hasan, A., Ding, C., ... & Geng, T. (2023, July). Ising-cf: A pathbreaking collaborative filtering method through efficient ising machine learning. In *2023 60th ACM/IEEE Design Automation Conference (DAC)* (pp. 1-6). IEEE.
- [21] John C. Duchi;Elad Hazan;Yoram Singer. Adaptive Subgradient Methods for Online Learning and Stochastic Optimization. *Journal of Machine Learning Research*, vol. 12 2011. PP 2121-2159, July 2011.
- [22] Hui Zou,Trevor Hastie.*Journal of the Royal Statistical Society. Series B (Statistical Methodology)*Regularization and Variable Selection via the Elastic Net. vol. 67 , Issue 2. 2005. PP 301-320, October 2005.
- [23] Guo, A., Hao, Y., Wu, C., Hagi, P., Pan, Z., Si, M., ... & Geng, T. (2023, June). Software-hardware co-design of heterogeneous SmartNIC system for recommendation models inference and training. In *Proceedings of the 37th International Conference on Supercomputing* (pp. 336-347).
- [24] Dai, W., Tao, J., Yan, X., Feng, Z., & Chen, J. (2023, November). Addressing Unintended Bias in Toxicity Detection: An LSTM and Attention-Based Approach. In *2023 5th International Conference on Artificial Intelligence and Computer Applications (ICAICA)* (pp. 375-379). IEEE.
- [25] Xin Chen , Yuxiang Hu, Ting Xu, Haowei Yang, Tong Wu. (2024). Advancements in AI for Oncology: Developing an Enhanced YOLOv5-based Cancer Cell Detection System. *International Journal of Innovative Research in Computer Science and Technology (IJRCST)*, 12(2),75-80, doi:10.55524/ijrcst.2024.12.2.13.
- [26] Mateusz Buda,Atsuto Maki,Maciej A. Mazurowski. A systematic study of the class imbalance problem in convolutional neural networks. *Neural Networks*, vol. 106. PP 249-259, August 2018.
- [27] Yulu Gong , Haoxin Zhang, Ruilin Xu, Zhou Yu, Jingbo Zhang. (2024). Innovative Deep Learning Methods for Precancerous Lesion Detection. *International Journal of Innovative Research in Computer Science and Technology (IJRCST)*, 12(2),81-86, doi:10.55524/ijrcst.2024.12.2.14.
- [28] Maryam Hamidi,Hassan Ghassemani,Maryam Imani. Classification of heart sound signal using curve fitting and fractal dimension. *Biomedical Signal Processing and Control*, vol. 39 2018. PP 351-359, January 2018.
- [29] Bradley M Whitaker,Pradyumna B Suresha,Chengyu Liu,Gari D Clifford,David V Anderson. Combining sparse coding and time-domain features for heart sound classification. *Physiological Measurement*, vol. 38 , Issue 8. 2017. PP 1701-1713, August 2017.
- [30] Wenjie Zhang,Jiqing Han,Shiwen Deng. Heart sound classification based on scaled spectrogram and tensor decomposition. *Expert Systems With Applications*, vol. 84. PP 220-231, January 2017.
- [31] Liu, Y., Yang, H., & Wu, C. (2023). Unveiling patterns: A study on semi-supervised classification of strip surface defects. *IEEE Access*, 11, 119933-119946.
- [32] Li, S., Kou, P., Ma, M., Yang, H., Huang, S., & Yang, Z. (2024). Application of Semi-supervised Learning in Image Classification: Research on Fusion of Labeled and Unlabeled Data. *IEEE Access*.
- [33] Yan, X., Xiao, M., Wang, W., Li, Y., & Zhang, F. A Self-Guided Deep Learning Technique for MRI Image Noise Reduction. *Journal of Theory and Practice of Engineering Science*, vol. 4, pp. 109-117, January 2024.
- [34] Wang, X. S., & Mann, B. P. (2020). Attractor Selection in Nonlinear Energy Harvesting Using Deep Reinforcement Learning. *arXiv preprint arXiv:2010.01255*.
- [35] Hu, Z., Li, J., Pan, Z., Zhou, S., Yang, L., Ding, C., ... & Jiang, W. (2022, October). On the design of quantum graph convolutional neural network in the nisq-era and beyond. In *2022 IEEE 40th International Conference on Computer Design (ICCD)* (pp. 290-297). IEEE.
- [36] Christian Szegedy;Wei Liu 0015;Yangqing Jia;Pierre Sermanet;Scott E. Reed;Dragomir Anguelov;Dumitru Erhan;Vincent Vanhoucke;Andrew Rabinovich. Going Deeper with Convolutions. *CoRR*, vol. 1409.4842 2014, March 2014.
- [37] Hao Xu, Shuang Song, and Ze Mao. 2023. Characterizing the Performance of Emerging Deep Learning, Graph, and High Performance Computing Workloads Under Interference. *arXiv:2303.15763*
- [38] Yoo, D., & Kweon, I. S. (2019). Learning loss for active learning. In *Proceedings of the IEEE/CVF conference on computer vision and pattern recognition* (pp. 93-102).